HHS Public Access

Author manuscript

J Alzheimers Dis. Author manuscript; available in PMC 2017 January 28.

Published in final edited form as:

J Alzheimers Dis. 2017 ; 56(2): 743–761. doi:10.3233/JAD-161027.

Quantitative Comparison of Dense-Core Amyloid Plaque Accumulation in Amyloid-β Precursor Protein Transgenic Mice

Peng Liu[a,b], **John H. Reichl**[a,b], **Eshaan R. Rao**[b,e], **Brittany M. McNellis**[b,e], **Eric S. Huang**[a,b], **Laura S. Hemmy**[c,f], **Colleen L. Forster**[b,d], **Michael A. Kuskowski**[c], **David R. Borchelt**[g], **Robert Vassar**[h], **Karen H. Ashe**[a,b,e,f], and **Kathleen R. Zahs**[a,b,*]

[a]Department of Neurology, University of Minnesota, Minneapolis, MN 55455

[b]N. Bud Grossman Center for Memory Research and Care, University of Minnesota, Minneapolis, MN 55455

[c]Department of Psychiatry, University of Minnesota, Minneapolis, MN 55455

[d]UMN Academic Health Center Biological Materials Procurement Network, University of Minnesota, Minneapolis, MN 55455

[e]Department of Neuroscience, University of Minnesota, Minneapolis, MN 55455

[f]GRECC, VA Medical Center, Minneapolis, MN 55417

[g]Department of Neuroscience, University of Florida, Gainesville, FL 32610

[h]Department of Cellular and Molecular Biology, Feinberg School of Medicine, Northwestern University, Chicago, IL 60611

Abstract

There exist several dozen lines of transgenic mice that express human amyloid-β precursor protein (AβPP) with Alzheimer's disease (AD)-linked mutations. AβPP transgenic mouse lines differ in the types and amounts of Aβ that they generate and in their spatiotemporal patterns of expression of Aβ assemblies, providing a toolkit to study Aβ amyloidosis and the influence of Aβ aggregation on brain function. More complete quantitative descriptions of the types of Aβ assemblies present in transgenic mice and in humans during disease progression should add to our understanding of how Aβ toxicity in mice relates to the pathogenesis of AD. Here, we provide a direct quantitative comparison of amyloid plaque burdens and plaque sizes in four lines of AβPP transgenic mice. We measured the fraction of cortex and hippocampus occupied by dense-core plaques, visualized by staining with Thioflavin S, in mice from young adulthood through advanced age. We found that the plaque burdens among the transgenic lines varied by an order of magnitude: at 15 months of age, the oldest age studied, the median cortical plaque burden in 5XFAD mice was already ~4.5 times that of 21-month Tg2576 mice and ~15 times that of 21–24-month rTg9191 mice. Plaque-size distributions changed across the lifespan in a line- and region-dependent manner. We also compared the dense-core plaque burdens in the mice to those

*Corresponding author: Kathleen R. Zahs, N. Bud Grossman Center for Memory Research and Care, 5-184 Wallin Medical Biosciences Building, 2101 6th Street SE, Minneapolis, MN 55455, zahsx001@umn.edu, Phone (612) 624-9985, FAX (612) 626-2639.

measured in a set of pathologically-confirmed AD cases from the Nun Study. Cortical plaque burdens in Tg2576, $APP_{Swe}PS1\Delta E9$, and 5XFAD mice eventually far exceeded those measured in the human cohort.

Keywords

Amyloid plaque; Amyloid-β precursor protein; Transgenic mouse; Alzheimer's disease; Thioflavin S; Plaque burden; Plaque size

Introduction

There currently exist more than 50 lines of transgenic mice that express human amyloid-β precursor protein (AβPP) with Alzheimer's disease (AD)-linked mutations [1]. Many of these lines display cognitive deficits and neuropathological features of AD (e.g., amyloid plaques, plaque-associated neuritic abnormalities, synapse loss), although they do not generate neurofibrillary tangles or suffer the widespread neuron loss characteristic of the human disease. While AβPP transgenic mice are incomplete disease models, they may be used to elucidate mechanisms of Aβ generation, aggregation, clearance, and toxicity. The various AβPP transgenic mouse lines differ in the types and amounts of Aβ that they generate and in their spatiotemporal patterns of expression of Aβ assemblies (for examples, see [2–4]). Thus, the phenotypic abnormalities seen across lines may result from different toxic agents and mechanisms of action. Additionally, the choice of line and age can markedly influence experimental results and interpretations. This was recently illustrated by a series of studies examining the effects of genetic ablation of TREM2 (triggering receptor expressed on myeloid cells) on Aβ accumulation in the brains of AβPP transgenic mice. Genome-wide association studies had identified rare variants of TREM2 that can as much as triple one's risk of developing AD [5, 6], stimulating a great deal of interest in the role of TREM2 in regulating Aβ pathology. TREM2 deletion was found to *decrease* hippocampal Aβ plaque accumulation in APPPS1-21 mice examined at 4 months of age, suggesting that TREM2 facilitates amyloid accumulation [7]. Conversely, 8-month 5XFAD mice deficient in TREM2 showed *increased* hippocampal Aβ plaque accumulation, suggesting that TREM2 protects against amyloid pathology [8]. Interestingly, both studies agreed that TREM2 deletion does not affect cortical plaque accumulation. Wang et al. hypothesized that the difference in the ages of the mice at the time of analysis might account for the discrepancy between the studies regarding hippocampal Aβ accumulation [9] and that the kinetics of plaque deposition might account for the apparent regional differences [8]. While these apparently contradictory findings do not clarify the influence of TREM2 on Aβ pathology, they do highlight the need for increased understanding of how features of AβPP transgenic mice vary with line and age.

As a step towards achieving this goal, we and others have undertaken comparisons of Aβ species generated in different AβPP transgenic mice. Employing immunoprecipitation followed by mass spectrometry, a group from the Spanish biotech company Araclon recently identified 39 species of Aβ peptides in the brains of $APP_{Swe}PS1\Delta E9$ mice, many of which were N-terminally truncated, but only 10 species in the brains of Tg2576 mice [2]. Here, we

present a quantitative description of the age-dependent accumulation of dense-core plaques in the brains of four lines of transgenic mice: $APP_{Swe}PS1\Delta E9$ [10], 5XFAD [11], and Tg2576 [12], among the most popular lines in use today, and rTg9191, a recently-developed line that generates only plaques and plaque-associated oligomers [4, 13]. (A PubMed search using keywords "amyloid plaques" and "mouse," but excluding reviews, returned 1204 papers published between January 2013 and July 2016. Of these, 721 studies examined amyloid pathology in mice. $APP_{Swe}PS1\Delta E9$, 5XFAD, and Tg2576 contributed 142 (17%), 101 (12%), and 83 (10%), respectively, of the 816 instances where mouse lines modeling amyloid pathology were identified.)

We surveyed the tissue banks of the laboratories that created these lines, and were able to obtain brain specimens from animals prior to ($APP_{Swe}PS1\Delta E9$, rTg9191, Tg2576) or near the age of onset (5XFAD) of plaque deposition through late-middle (15–17 months; 5XFAD, $APP_{Swe}PS1\Delta E9$) to old (21–24 months; rTg9191, Tg2576) age. Because the kinetics of plaque deposition have been reported to be gender-dependent [13–16], we selected cohorts containing only a single gender within each line; with this criterion, we had available tissue from female 5XFAD mice and from male mice of the other three lines. We elected to proceed with this study with the tissue currently available, as gender is only one among several factors that can influence plaque deposition or AβPP metabolism, including background strain [17], housing conditions [18, 19] and even maternal diet [20] or activity [21].

We focused on dense-core plaques, as these lesions have been shown to be centers of neuroinflammatory responses [22–24], and structural [25–30] and functional [31–33] neuronal and glial abnormalities. Using stereology-based methods, we quantified dense-core plaque burdens (areal fraction occupied by plaques) in the cortex and hippocampus of young, middle-aged, and old mice, and compared these values with plaque burdens in the frontal, temporal, and parietal cortices of pathologically-confirmed AD cases. In addition, we measured plaque sizes in the mice, as microglial responses [34] and degree of plaque-associated neuritic abnormalities [35] have been reported to correlate with plaque size.

We found that the dense-core plaque burdens among the transgenic lines varied by an order of magnitude and that plaque-size distributions changed across the lifespan in a line- and region-dependent manner.

Materials and Methods

Collection and preparation of mouse brain sections

Tg2576 [12] and rTg9191 [13] mice were bred and aged at the University of Minnesota, Minneapolis, MN. Mice were anesthetized using isoflurane and killed by decapitation. Brains were harvested and the left hemispheres were immediately immersion-fixed in 10% (v/v) formalin for 24–48 hours, then embedded in paraffin. 5XFAD mice were bred and aged at Northwestern University, Chicago, IL; brains of these mice were fixed with 4% (w/v) paraformaldehyde (PFA), then cryopreserved in 30% (w/v) sucrose/PBS, and stored at 4°C prior to shipping to the University of Minnesota for further processing. When the brains arrived in Minnesota, they were embedded in paraffin. Paraffin-embedded brains were

serially sectioned at 7 μm in the parasagittal plane using a Leica RM2255 Fully Motorized Rotary Microtome (Leica™ Microsystems, Buffalo Grove, IL); sections were mounted onto Fisher Super Frost Plus slides (Fisher Scientific, Pittsburgh, PA), then deparaffinized and rehydrated according to standard protocols. Sagittal sections (6–7 μm) of $APP_{Swe}PS1\Delta E9$ mice (2, 11, and 17 months of age) were prepared at the University of Florida, Gainesville, FL and sent to the University of Minnesota, where they were deparaffinized and rehydrated before Thioflavin S (ThioS) staining. Additionally, 8-month $APP_{Swe}PS1\Delta E9$ mice were provided by Dr. James Cleary of the Minneapolis Veterans Administration Medical Center; tissue from these mice was harvested and processed as for the Tg2576 and rTg9191 mice.

Two to six mice per line per age (see Table 1, Supplementary Table 1) were studied. All experiments involving mice were conducted in full accordance with the Association for Assessment and Accreditation of Laboratory Animal Care (AAALAC) guidelines and approved by the local Institutional Animal Care and Use Committees (IACUC).

Human brain tissue

Samples of brain tissue from subjects exhibiting clinical and neuropathological characteristics of AD were obtained from the Nun Study [36, 37]. Informed consent for evaluation and autopsy was obtained from all individual participants included in the Nun Study at the time of enrollment and periodically throughout the longitudinal follow-up. Procedures were conducted in accord with the Helsinki Declaration of 1975 and approved by the Institutional Review Boards of the University of Kentucky and the University of Minnesota. Selection criteria included: 1) objective cognitive and functional evaluation consistent with dementia, 2) CERAD semi-quantitative neuritic plaque score “C,” and 3) Braak stage 5 or 6. The 60 cases that met these criteria were divided into tertiles based on neocortical neuritic plaque numbers (mean number of neuritic plaques/mm^2 in sections of frontal lobe, superior and middle temporal gyrus, and inferior parietal lobe), and two cases were chosen from each tertile. Characteristics of the selected subjects are summarized in Table 2. Three formalin-fixed tissue blocks – taken from frontal lobe (area 9), superior and middle temporal gyrus, and inferior parietal lobe – were collected for each subject. Blocks were embedded in paraffin and sectioned at 7 μm. Sections were mounted, deparaffinized, and rehydrated, as for the mouse brain sections, then stained with ThioS.

Detection of dense-core Aβ plaques

To reveal dense-core amyloid plaques, deparaffinized and rehydrated brain sections were briefly rinsed in ddH_2O, and then incubated in freshly prepared 1% (w/v) ThioS (Sigma-Aldrich, St. Louis, MO) aqueous solution at room temperature for 5 minutes followed by differentiation using 70% ethanol for 5 minutes. Sections were then briefly rinsed in ddH_2O, and cover-slipped with aqueous mounting media (Vectashield, Vector Laboratories, Burlingame, CA).

Quantification of amyloid burden

Amyloid plaques were viewed with an Axio Imager upright microscope (Carl Zeiss Microimaging GmbH, Göettingen, Germany) equipped with an AxioCam MRm monochrome digital camera for capturing images of ThioS-reactive plaques. Stereology-

based quantification of amyloid burden was carried out using the area fraction fractionator module in Stereo Investigator 10 software (MBF Bioscience, Chicago, IL). The entire cerebral cortex and hippocampus were separately sampled with the counting frame size of 180 μm × 180 μm and grid size of 100 μm^2. For the transgenic mice, we quantified 60 frames per section in cortex, and 35 frames per section in hippocampus. The sum of the area of all ThioS-reactive plaques was divided by the total area of cerebral cortex or hippocampus to obtain the amyloid burden (total area: range 4.1–10.3 mm^2 for cortex and 1.1–3.6 mm^2 for hippocampus). For the human tissue, we studied 48 frames per section per region of interest; amyloid burden was again calculated as the area of all ThioS-reactive plaques divided by the total area sampled (total area: range 165–375 mm^2). Amyloid burden was quantified in 2–6 sections per mouse brain and in 2–4 sections/region/subject for human samples. Experimenters performing the quantification were blind to age and transgenic line of mice, and to cortical region and plaque-density for the human samples.

Measurement of plaque sizes

Plaque areas were measured in 7-μm thick sagittal sections, viewed under epifluorescence illumination at 20× on the Axio Imager microscope. Plaque sizes were determined using the nucleator module of the Stereo Investigator software. The center of each plaque was marked manually and orthogonal lines radiating from this center were generated by the software. The points of intersection of these lines with the plaque edge were marked manually, and the area of the ellipse formed with these line segments as the major and minor axes was calculated by the software. Plaques were measured in two sections from three animals at each age for each line. The number of plaques sampled varied with line and age. In cases where plaque burdens were very low (e.g., Tg2576 and rTg9191 mice around the age of onset of plaque deposition), we measured every plaque in hippocampus and cortex. For sections with high plaque burdens, we initially employed systematic sampling over entire regions (cortex or hippocampus) as described above for plaque burdens, and measured every plaque in the counting frame. We conducted an interim analysis of these data to determine whether setting a criterion number of plaques (100 plaques per line-age-region) would yield results similar to the more exhaustive data collection. Data sets (line-age-region) containing >250 plaques (7 data sets) were identified, and cumulative probability plots of plaque-size distributions were created. Then 100 plaques were randomly selected from each data set and a new cumulative probability plot was constructed; 10 iterations were carried out. For each line-age-region, the plaque-size distribution for the complete data set was compared to the distribution for each set of 100 randomly selected plaques, using the Kolmogorov-Smirnov test. In all cases, the distributions of the complete and partial data sets were similar ($p > 0.15$). In addition, for each line-age-region, all of the partial data sets were similar to each other (Kruskal-Wallis test). We therefore set a goal of measuring ~100 plaques/transgenic line-age-region, distributed among three animals.

We also evaluated an alternative method for measuring plaque areas, in an attempt to accelerate data collection. Images of entire ThioS-stained sections were generated using a Nikon TiE deconvolution microscope system (Nikon Instruments Inc., Melville, NY) at the University of Minnesota Imaging Center; sections were scanned at low magnification (10× objective) and fields were tiled with 5% overlap. These images were then analyzed with

ImageJ software. Images first were manually edited to remove edge artifacts, folds, and blood vessels, then subjectively thresholded. Regions of interest (cortex, hippocampus) were outlined and the automatic particle-size feature was used to measure the areas of all bright objects (presumably ThioS-stained plaques) within the regions. As described below in *Results*, the particle-size distributions obtained with this method greatly differed from the plaque-size distributions obtained using the more time-consuming, but more accurate, measurement of plaques viewed at higher magnification on the Axio Imager microscope. Therefore, the plaque areas reported here were those obtained using Stereo Investigator software to measure plaques viewed on the Axio Imager microscope, as described above.

Statistics

For plaque burdens, descriptive statistics (median, interquartile ranges, minimum and maximum values, for each line and age) were calculated, using each section as a data point. Non-parametric analyses of variance and post-hoc tests (Kruskal-Wallis tests; followed by Mann-Whitney tests) were used to compare plaque burdens within or between lines; p-values were Bonferroni-adjusted within the families of two-group comparisons (i.e., between ages within a line, or between lines within an age group).

For plaque areas, descriptive statistics (median, interquartile ranges, minimum and maximum values, for each line and age) were calculated using each plaque as a data point. In addition, cumulative probability plots (empirical cumulative distribution functions) were generated for each line-age-region. Kolmogorov-Smirnov tests were used to compare distributions, and p-values were Bonferroni-adjusted within the families of two-group comparisons.

Imaging of brain sections

Photomicrographs of the ThioS-stained brain sections were generated using a Nikon TiE deconvolution microscope system at the University of Minnesota Imaging Center. The intensities of the images were adjusted in PhotoShop in order to visualize the outlines of the sections. Images are presented with contrast inverted.

Results

ThioS, which binds to amyloid fibrils with β-sheet structure, was used to reveal dense-core plaques in the brains of AβPP transgenic mice and of AD cases.

Plaque burden

The transgenic mice studied here varied greatly in the age of onset and amount of plaque deposition. As expected, plaque deposition occurred earlier and to a much greater extent in the two lines that express *Presenilin-1* transgenes in addition to *AβPP* transgenes. ThioS-positive plaques were already apparent in 3-month 5XFAD mice. In both cortex and hippocampus, plaque burdens increased throughout the animals' first year, then plateaued between 12 and 15 months of age (Figs. 1,3). (See Table 3 for results of the analysis of variance and post-hoc tests.) Median plaque burdens reached 6.1% (range: 5.1–7.6%) in

cortex and 4.8% (range: 2.4–5.7%) in hippocampus at 15 months, the oldest age studied in this line. (See Supplementary Table 1 for descriptive statistics for all lines and ages.)

Among the $APP_{Swe}PS1\Delta E9$ mice studied here, ThioS-positive plaques were first observed in the 8-month cohort. However, we did not examine any mice between two and eight months of age. Cortical and hippocampal plaque burdens continued to increase with age until at least 17 months, the oldest age studied in this line (Figs. 1,3; Table 3). At 17 months of age, median cortical and hippocampal plaque burdens in $APP_{Swe}PS1\Delta E9$ mice were 3.8% (range: 1.1–5.6%) and 2.8% (range: 1.4–7.5%), respectively.

Plaque deposition began later and was less extensive in the two lines that expressed only an AβPP transgene. ThioS-positive plaques appeared in cortex and hippocampus of rTg9191 mice at 12–14 months. Plaque burden in the cortex increased through at least 21–24 months, the oldest ages studied (Figs. 2,3; Table 3). In the hippocampus, there was a trend towards increasing plaque burden through 21–24 months, but the difference between 14–17-month and 21–24-month animals was not significant when p values were adjusted for multiple comparisons. Median plaque burdens reached only 0.3% (range: 0.2–0.5%) and 0.2% (range: 0.1–0.6%) in the cortex and hippocampus, respectively, at 21–24 months.

In Tg2576 mice, ThioS-positive plaques first appeared in the cortex between 10 and 13 months of age, and their levels plateaued between 16 and 21 months. In the hippocampus, ThioS plaques were first observed between 13 and 16 months, and plaque burden increased at least through 21 months, the oldest age studied in this line (Figs. 2,3; Table 3). Median plaque burdens reached 1.4% (range: 0.6–3.0%) and 0.8% (range: 0.5–1.6%) in cortex and hippocampus, respectively, at 21 months.

We next compared the age-dependent ThioS-positive plaque burdens between lines. Because the different lines were evaluated at different ages, ages were binned into 4–5-month intervals across the lifespan (results of statistical analyses are reported in Supplementary Table 2). Cortical plaque burdens were highest in 5XFAD at all ages studied. In the hippocampus, 5XFAD burdens were higher than those of rTg9191 or Tg2576 at all ages, and higher than those of $APP_{Swe}PS1\Delta E9$ at 2–5 months (prior to the appearance of dense-core plaques in the animals studied here) and 10–13 months (there was a tendency towards larger plaque burden in 5XFAD compared to $APP_{Swe}PS1\Delta E9$ at 6–9 months, but this difference did not reach statistical significance when p values were adjusted for multiple comparisons). It should be recalled that the 5XFAD mice used in this study were females, while the mice from the other lines were males. Plaque burdens in cortex and hippocampus of $APP_{Swe}PS1\Delta E9$ were greater than those of rTg9191 and Tg2576 at all ages. Plaque burdens in cortex and hippocampus of Tg2576 exceeded those of rTg9191 at 14–17 months and 21–23 months.

Finally, we compared plaque burdens between lines based on duration of plaque deposition (results summarized in Table 4). We observed ThioS-positive plaques at 3 months of age in the cortex and hippocampus of 5XFAD mice, the earliest age we had available, but others have reported ThioS-positive plaques as early as 2 months of age [11]. ThioS-positive plaques have been observed in male $APP_{Swe}PS1\Delta E9$ mice as early as 4 months of age [38].

Dense-core plaques emerge in the cortex and hippocampus of male rTg9191 mice at ~12 months of age ([13] and current study). In the current study, we observed ThioS-positive plaques in the cortex of male Tg2576 mice at 10 months of age, but such plaques have been reported as early as 9 months (gender unspecified) [39]; in the hippocampus, ThioS-positive plaques emerged between 13 and 16 months (current study).

After 4 (±1) months of plaque deposition, the cortical plaque burdens were similar in 5XFAD (6M) and $APP_{Swe}PS1\Delta E9$ (8M), and the burdens in these two lines exceeded those in rTg9191 (17M) and Tg2576 (13M) (the latter two lines were similar to each other). In the hippocampus, the plaque burdens in 5XFAD (6M) and $APP_{Swe}PS1\Delta E9$ (8M) were again similar to each other; 5XFAD > Tg2576 (21M) > rTg9191 (17M); $APP_{Swe}PS1\Delta E9$ > Tg2576, but did not differ significantly from rTg9191 when the p value was adjusted for multiple comparisons.

After 12 (±1) months of plaque deposition, the cortical plaque burden was highest in 5XFAD (15M), intermediate in $APP_{Swe}PS1\Delta E9$ (17M), and lowest in Tg2576 (21M). Hippocampal plaque burdens did not differ between 5XFAD and $APP_{Swe}PS1\Delta E9$. Data were not available for rTg9191 (either region) or for hippocampal plaque burden in Tg2576 mice following a year of plaque deposition.

In summary, dense-core plaque burdens differed among the transgenic mouse lines by more than an order of magnitude. At 15 months of age, the oldest age studied, the median cortical plaque burden in 5XFAD mice was already ~4.5 times that of 21-month Tg2576 mice and ~15 times that of 21–24-month rTg9191 mice.

Human

In order to assess how dense-core plaque burdens in mice compare to those in AD brains, we also measured plaque burdens in a group of autopsy specimens from the Nun Study, using the same methods that we applied to the mouse samples. The ThioS-positive plaque burdens in frontal lobe, superior and middle temporal gyrus, and inferior parietal lobe were determined for six AD cases (Table 2). These cases were selected to span the range of neuritic plaque densities (number of plaques per unit area in Bielschowsky-stained sections) seen in subjects with clinical and neuropathological features of AD in this cohort. The composite cortical ThioS plaque burdens (plaque burdens averaged over the three regions for each subject) ranged from 0.06% to 0.37%. In this small sample, there did not emerge a consistent regional hierarchy of plaque deposition within individuals: in three subjects, the highest plaque burdens were measured in the inferior parietal lobes; in two subjects, the frontal lobe; and in the sixth subject, the superior and middle temporal gyrus.

Three of the four transgenic mouse lines studied here exhibited median cortical dense-core plaque burdens that exceeded the maximum composite cortical plaque burden measured in the AD cases from the Nun Study. This occurred by 3 months of age in 5XFAD mice, by 8 months in $APP_{Swe}PS1\Delta E9$ mice, and by 16 months in Tg2576 mice. Plaque burdens in the 5XFAD and $APP_{Swe}PS1\Delta E9$ eventually reached levels that were an order of magnitude higher than the composite cortical plaque burdens in the human samples, and the cortical plaque burden in 21-month Tg2576 mice, the oldest age studied, was ~twice that of the

human AD cases. The cortical plaque burden in rTg9191 mice remained within the range observed in AD brains, even at 21 months, the oldest age studied in these mice.

Plaque size

ThioS-stained sections were viewed on Axio Imager microscope and plaque areas were measured using Stereo Investigator software, as described in **Materials and Methods**. Plaque areas were found to be lognormally distributed and are displayed as cumulative probability plots in Figures 4–5 and Supplementary Figure 1. (For alternative graphical representations of these data, see the histograms in Supplementary Figures 2–4. Descriptive statistics are presented in Supplementary Table 3.)

We first analyzed age-related alterations in plaque size for each mouse line. For cortical plaques in 5XFAD mice, the distributions exhibit a rightward shift between 3 and 9 months of age, but the distribution at 12 months is similar to that at 9 months, while the 15-month distribution shifts leftward and is similar to that of 6-month mice (Fig. 4A, Table 5). Plaque-size distributions in the hippocampus also shift rightwards between 3 and 9 months, with the distributions at 12 and 15 months falling between those at 6 and 9 months (Fig. 4B, Table 5). This pattern of change in the size distributions is consistent with plaque growth between 3 and 9 months of age, followed by plaque shrinkage between 12 and 15 months.

In $APP_{Swe}PS1\Delta E9$ mice, cortical plaque-size distributions differed between 8-month and 17-month mice, showing a rightward shift with age in the lower ~2/3 of the distribution (Fig. 4C, Table 5). This change in the shape of the cumulative probability plot could occur if plaques reach a maximum size by 8 months of age, but small plaques continue to be added to the population. Hippocampal plaque-size distributions were similar for 8-, 11-, and 17-month $APP_{Swe}PS1\Delta E9$ mice (Fig. 4D, Table 5).

For rTg9191 cortex (Fig. 4E) and hippocampus (Fig. 4F), the cumulative probability distributions appeared to show a rightward shift between 12 and 17 months, with no further changes between 17 and 21 months. However, when p values were adjusted for multiple comparisons, neither the cortical nor hippocampal distributions changed significantly as a function of age (Table 5). It should be noted that a relatively small number of plaques were measured in this line, which displayed the lowest plaque burden among the lines studied here. For Tg2576 mice, cortical plaque-size distributions shifted rightwards between 13 and 21 months of age (Fig. 4G, Table 5). Hippocampal plaque sizes were measured at only two ages in this line, and there was a rightward shift in the curves between 16 and 21 months (Fig. 4H, Table 5).

As for plaque burden, we also compared plaque sizes between lines, based on age (Supplementary Figs. 1,3 and Supplementary Table 4) and on duration of plaque deposition (Fig. 5, Supplementary Fig. 4, and Table 6). At 6–9 months of age, the size distributions of both cortical and hippocampal plaques differed between 5XFAD and $APP_{Swe}PS1\Delta E9$ mice, but the relationship was not simple. In the cortex, $APP_{Swe}PS1\Delta E9$ had smaller plaques than 5XFAD in the lower ~80% of the distribution, but larger plaques in the upper ~20%; in the hippocampus, $APP_{Swe}PS1\Delta E9$ had smaller plaques in the lower ~half of the distribution, but similarly-sized plaques in the upper half (Supplementary Figs. 1A,B; Supplementary Table

4). rTg9191 and Tg2576 mice had not yet deposited dense-core plaques at this age. Between 10 and 13 months of age, the cortical plaque-size distribution of 5XFAD differed from that of the other three lines, showing a rightward shift compared to rTg9191 and Tg2576, while the plots for 5XFAD and $APP_{Swe}PS1\Delta E9$ crossed at ~0.6 cumulative probability. The cortical distribution for $APP_{Swe}PS1\Delta E9$ was also shifted to the right compared to rTg9191 and Tg2576. Tg2576 and rTg9191 did not differ from each other at this age (Supplementary Fig. 1C; Supplementary Table 4). In the hippocampus, 5XFAD had larger plaques than rTg9191; although there was a trend towards larger plaques in $APP_{Swe}PS1\Delta E9$ compared to rTg9191, the p value did not reach significance when corrected for multiple comparisons (Supplementary Fig. 1D; Supplementary Table 4). ThioS-positive plaques were not detected in the hippocampus of Tg2576 at this age. By 14–17 months, plaque-size distributions in cortex were similar among the lines, with the exception of rTg9191, which tended to have smaller plaques (Supplementary Fig. 1E; Supplementary Table 4); the relationship between hippocampal plaque-size distributions was more complex, with the curves crossing each other (Supplementary Fig. 1F; Supplementary Table 4). Finally in the oldest age group (21–24M), cortical and hippocampal plaque sizes differed between rTg9191 and Tg2576 mice; plaques tended to be larger in Tg2576 (Supplementary Figs. 1G,H; Supplementary Table 4).

When plaque-size distributions were compared based upon duration of plaque deposition, the relationship between lines was again complex. After 3–5 months of plaque deposition in the cortex, the plaque-size distribution in rTg9191 did not significantly differ from any of the other lines (Fig. 5A, Table 6). The distribution for $APP_{Swe}PS1\Delta E9$ differed only from 5XFAD, but the relationship was not simple, with crossing of the cumulative probability curves for the two lines (Fig. 5A, Table 6). Tg2576 also differed only from 5XFAD, showing a general leftward shift in the cumulative probability distribution (i.e., smaller plaques in Tg2576) (Fig. 5A, Table 6). However, in hippocampus, the plaque-size distribution in Tg2576 was shifted to the right over much of its extent compared to the distribution for 5XFAD (i.e., hippocampal plaques tended to be larger in Tg2576) (Fig. 5B, Table 6). It should be noted that some of the largest areas in Tg2576 mice actually represented clusters of plaques where multiple cores were visible but borders between plaques could not be differentiated. We had the impression that such clusters were more frequent in Tg2576 than in the other lines. The difference between the plaque-size distributions in 5XFAD and Tg2576 was the only statistically significant difference among the hippocampal distributions after 4±1 months of plaque deposition. After a year of plaque deposition, cortical plaques in Tg2576 mice were larger than those in 5XFAD or $APP_{Swe}PS1\Delta E9$ mice (data were not available from rTg9191) (Fig. 5C, Table 6), and the size distributions in hippocampus differed between 5XFAD and $APP_{Swe}PS1\Delta E9$ – $APP_{Swe}PS1\Delta E9$ had smaller plaques in the lower ~half of the distribution, but similarly-sized plaques in the upper half (Fig. 5D, Table 6).

Comparison of methods for measuring plaque sizes

Viewing sections at relatively high magnification permits the unequivocal identification of ThioS-stained plaques, but can be quite time-consuming, requiring the sampling of many fields. Seeking a method that would allow us to rapidly measure all of the plaques within a region of interest (e.g., hippocampus, cortex), we subjected low-magnification images to an

automated particle-size analysis, as described in **Materials and Methods**. Most sections contained small autofluorescent profiles that clearly were not plaques, so we first determined a lower-size limit for including particles in the analysis. Particles were measured in regions of sections that did not contain plaques (one section per line-age); 95% of these particles were smaller than 35 μm^2. Therefore, only particles larger than 35 μm^2 were included in the "plaque size" analysis. Nonetheless, the particle-size distributions obtained using the automated method were quite different than the plaque-size distributions obtained using our standard method, showing a significant leftward shift (i.e., many smaller particles in the automated analysis than in the standard plaque-size analysis) (Fig. 6; Supplementary Table 5). We concluded that the automated method did not allow the accurate measurement of plaque sizes.

DISCUSSION

Transgenic mice that express human AβPP provide a toolkit to study Aβ amyloidosis and the influence of Aβ aggregation on brain function. As different lines generate different types and amounts of Aβ assemblies in an age-dependent manner, the type of Aβ toxicity that predominates will vary between lines and even with age within a line. We here provide the first direct quantitative comparison of four lines of AβPP transgenic mice used to model amyloid toxicity, and show that dense-core plaque burdens vary by more than an order of magnitude between the lines.

The amount and kinetics of plaque deposition in each AβPP transgenic mouse could result from multiple factors, including genetic background, level of transgene expression, and Alzheimer's disease-linked mutation(s) in the transgene(s) that influence the (relative) amounts of Aβ isoforms generated by each line. Genetic background has been shown to influence AβPP metabolism [17] in transgenic mice, although we are unaware of any systematic investigations into the effect of background strain on amyloidosis in the lines studied here. The lines are reported to differ somewhat in the amount of transgenic AβPP expressed: Tg2576 mice express ~6 units (relative to the amount of endogenous mouse AβPP) of transgenic AβPP [12, 13]; rTg9191 express ~4 units [13]; APP_{Swe}PS1ΔE9 express 2–4 units [40], and 5XFAD express "slightly less" AβPP than Tg2576 [11]. In the former two lines, at least, AβPP expression does not change significantly with age [12, 13, 41]. The lines studied here differ in the transgenes that they carry (*AβPP* alone, or *AβPP* along with *presenilin-1*) and in the disease-linked mutations within these transgenes (Table 1). Together these differences affect the amount of $Aβ_{42}$ or the $Aβ_{42}/Aβ_{40}$ ratio, likely key determinants of Aβ aggregation. The "Swedish" mutation in AβPP (K670N, M671L), found in all four lines studied here, increases the production of total Aβ. The *AβPP* transgenes in 5XFAD and rTg9191 contain additional mutations that specifically promote the formation of $Aβ_{42}$ (the "London" (V717I) mutation in rTg9191, and the "London" and "Florida" (I716V) mutations in 5XFAD). Furthermore, 5XFAD and APP_{Swe}PS1ΔE9 carry transgenes encoding human presenilin-1 with mutations that increase the production of $Aβ_{42}$ relative to other Aβ peptides. (See [42] for a compendium of Alzheimer's disease-linked mutations.) Values for the $Aβ_{42}/Aβ_{40}$ ratio for each of the lines studied here can be found in, or derived from, the literature, although differences in methods used to extract and measure Aβ make it difficult to directly compare the results of the various studies. With that caveat in mind, $Aβ_{42}/Aβ_{40}$

was found to reach 25 in young 5XFAD mice, compared to a maximum value of ~0.2 in Tg2576 mice (guanidine HCl-extractable Aβ [11]). This ratio reached 1.3 in $APP_{Swe}PS1\Delta E9$, compared to ~0.3 in mice that expressed only the *APP_{Swe}* transgene (detergent-extractable Aβ [40]). In rTg9191 mice, the $A\beta_{42}/A\beta_{40}$ ratio between 12 and 21 months of age was ~0.4 (pooled aqueous, detergent-containing, and formic-acid extracts [13]). Confirming the influence of the levels of $A\beta_{42}$ on plaque formation, it was found that the rate of deposition and the total amyloid burden were proportional to $A\beta_{42}$ levels in different lines of 5XFAD mice [11]. The propensity of Aβ to aggregate may be influenced not only by its C-terminus, but also by N-terminal truncations and modifications. It was recently reported that $APP_{Swe}PS1\Delta E9$ generate abundant N-terminally truncated and pyroglutamate-modified Aβ species that are not found in Tg2576, and it was suggested that the hydrophobic nature of these peptides might partially account for the aggressive plaque deposition in $APP_{Swe}PS1\Delta E9$ [2].

The dense-core plaque burdens reported here are comparable to those reported previously for 5XFAD mice. The ThioS-positive plaque burden in 14-week female 5XFAD was found to be ~0.7% (calculated from the data in [43]) and the burden of plaques stained with X-34, another stain for fibrillar Aβ, in 4-month mice (gender unspecified) was ~0.8% [9], close to the 0.5% ThioS burden that we found in 3-month female 5XFAD mice. In 6-month 5XFAD mice (both males and females used in this study), the ThioS burden has been reported as 2.5–3% [44], similar to the 3.6% that we found in 6–9-month female mice. Interestingly, Condello et al. reported that plaque sizes in 5XFAD mice plateau as early as 8 months of age [45]. This is consistent with our data suggesting plaque growth through 9 months, although our data indicate that there may be some degree of plaque shrinkage – or, more properly, a shift in the distribution of the plaque population to smaller sizes – between 12 and 15 months. To the extent that we can compare plaque burdens between genders, the value obtained here for ThioS-stained plaques in aged Tg2576 mice (21-month male, median burden 1.4%) is consistent with that reported earlier (~0.1–2.5% in 22-month females [46]). Similarly, our value for middle-aged $APP_{Swe}PS1\Delta E9$ mice (17-month male, median 3.8%) is like that reported for 19-month females (~2.5–5.5%) studied by the same group [46]. However, two other studies reported substantially smaller plaque burdens and plaque sizes in $APP_{Swe}PS1\Delta E9$ than were found here: plaque burdens in 8–12-month mice were ~0.13% – 0.22% in one study (gender unspecified) [47] and 0.05–0.1% in the second study [38], while mean plaque areas in the two studies were ~130 μm^2 and ~12–17 μm^2, respectively. (Compare these values to our findings of burdens of 1.2% in cortex and 0.5% in hippocampus in 8-month mice; 2.1% in cortex and 1.4% in hippocampus of 11-month mice. Median cortical and hippocampal plaque areas in 8-month mice were 296 μm^2 and 408 μm^2, respectively; and ~360 μm^2 in both regions in 11-month mice. Due to the skewed distributions, mean areas are even larger.) Yet, by visual inspection, (see the photomicrographs in Fig. 2 of [47] and Fig. 1 of the current study), the ThioS plaque burdens in the $APP_{Swe}PS1\Delta E9$ studied by us and by Garcia-Alloza et al. appear similar. It is possible that the differences in the quantitative findings between the current study and the studies of Garcia-Alloza et al. and Ruan et al. are due to different methods for measuring plaques. The other two groups employed a thresholding method to identify and measure plaques. As described in **Results**, when we attempted to use an automated method to

measure objects defined by thresholding (“ImageJ method”), the plaque-size distributions were very different from those obtained using the manual (“Stereo Investigator”) method. The former method yielded smaller particle-size distributions, probably due both to the inclusion of objects that were not actually plaques and to underestimating the sizes of real plaques if only the plaque cores, but not the plaque peripheries, were above the threshold. Finally, yet another study [35] reported larger ThioS-positive plaques in 12-month Tg2576 and $APP_{Swe}PS1\Delta E9$ (gender unspecified) mice than we found here (mean areas ~ double those found in the current study). The discrepancies between the various studies point to the necessity of employing consistent methods when attempting quantitative comparisons.

We also examined changes in plaque-size distributions as a function of age. Our cross-sectional study obviously can only describe changes in the plaque population, rather than changes in the sizes of individual plaques. (For example, a rightward shift in the cumulative probability plot with increasing age could be due to the growth of individual plaques over time or to the emergence of larger plaques as animals age.) Observations in living animals have revealed the growth of individual plaques over periods of weeks to months [48–51]. Plaque shrinkage has also been reported [48–50]. *In vivo* imaging of plaques over a 6-week period in Tg2576 mice showed the emergence and growth of plaques in 12-month animals, but not in 18-month mice [50]. These findings confirmed the results of an earlier study showing that plaque size was largely stable in 18-month Tg2576 mice [52]. We observed rightward shifts in the plaque-size distributions between 13 and 16 months and between 16 and 21 months in our cross-sectional analysis; it is possible that much of the change in plaque sizes in the latter interval took place prior to 18 months. It should be noted that, contrary to our findings, no significant changes in ThioS-positive plaque size were seen between 12 and 22 months of age in another histological study of Tg2576 mice [52]. Whether this discrepancy reflects differences in methodology or actual differences in the animals is not known.

Finally, we compared the cortical dense-core plaque burdens in the mice to dense-core plaque burdens in cortical tissue from six AD cases that were processed and analyzed using the same methods used for mouse samples. In Tg2576, $APP_{Swe}PS1\Delta E9$, and 5XFAD mice, cortical plaque burdens eventually far exceeded the maximum composite cortical plaque burdens measured in the human cohort. The small number of human subjects and unusual demographic (> 90 years of age and residing in a homogeneous religious community) limits our ability to draw general conclusions about the relative dense-core plaque burdens in mouse and AD brains. For comparison to our human AD cohort, we could find only a single report of ThioS plaque burden in a relatively large sample of community dwelling AD subjects. In that study, which examined the superior temporal sulcus, the ThioS plaque burden was 1.2 ± 0.2% (mean ± S.E.M., N = 62) [53]. Two smaller studies reported ThioS plaque burdens of 3.0 ± 0.3% (N = 6 [35]; N = 7 [54]) in inferior temporal gyrus. The latter study also measured ThioS plaque burdens in subjects with familial autosomal AD caused by *Presenilin-1* mutations (8 subjects with 5 different mutations) and found that the burden in these subjects, 3.5 ± 0.3%, did not differ significantly from the burden in the subjects with sporadic AD. All of these studies employed some sort of systematic random sampling, although the exact methods differed, and different methods of tissue preparation were employed between, and even within, studies. The large variation in dense-core plaque

burdens found in the different studies might reflect differences in the study cohorts, brain regions examined, or methods used. Although a comprehensive evaluation of dense-core plaque burdens in the general population of AD patients is beyond the scope of the current study, the values obtained here for human and mouse brain at least provide a consistent comparison using the same methods of tissue preparation and analysis.

There are several limitations of this study. First, we depended upon archived tissue, and thus were not able to completely age- and gender- match mice across lines. We therefore had to bin ages into 4–5 month intervals throughout the lifespan in order to compare pathology across transgenic lines. The numbers of animals for each line-age was small, due to tissue availability. For the estimates of plaque size, we measured plaque areas in thin sections, rather than plaque volumes in three dimensions. In comparing plaque-size distributions, we assumed that the sections intersected the plaques randomly and that the probability of cutting through any particular latitude (regarding plaques as spheres) was the same for all lines-ages. Despite these limitations, the current study provides the first direct quantitative comparison of dense-core plaque pathology as a function of age in three of the most popular AβPP transgenic mouse lines in use today.

The diversity among AβPP transgenic mice provides researchers the opportunity to dissect the effects of specific types of Aβ aggregates and AβPP metabolites on brain function. Yet this diversity can also lead to confusion when comparing results obtained in different lines or even at different ages within a line. More complete quantitative descriptions of the types of Aβ assemblies present in transgenic mice and in humans during disease progression should add to our understanding of how mechanisms of Aβ toxicity in mice relate to the pathogenesis of AD, and potentially increase the predictive validity of preclinical testing of potential AD therapies in AβPP transgenic mice.

Supplementary Material

Refer to Web version on PubMed Central for supplementary material.

Acknowledgments

This work was supported by the National Institute for Neurological Diseases and Stroke (R01 NS33249) (KHA) and the National Institute on Aging (R01 AG022560 (RV) and R01 AG009862 (Nun Study)) within the National Institutes of Health, and a gift from B. Grossman.

References

1. Alzforum, Research models. [Accessed March 31, 2015] http://www.alzforum.org/research-models.
2. Allue JA, Sarasa L, Izco M, Perez-Grijalba V, Fandos N, Pascual-Lucas M, Ogueta S, Pesini P, Sarasa M. Outstanding Phenotypic Differences in the Profile of Amyloid-beta between Tg2576 and APPswe/PS1dE9 Transgenic Mouse Models of Alzheimer's Disease. J Alzheimers Dis. 2016; 53:773–785. [PubMed: 27258422]
3. Kulnane LS, Lamb BT. Neuropathological characterization of mutant amyloid precursor protein yeast artificial chromosome transgenic mice. Neurobiol Dis. 2001; 8:982–992. [PubMed: 11741394]
4. Liu P, Reed MN, Kotilinek LA, Grant MK, Forster CL, Qiang W, Shapiro SL, Reichl JH, Chiang AC, Jankowsky JL, Wilmot CM, Cleary JP, Zahs KR, Ashe KH. Quaternary Structure Defines a

Large Class of Amyloid-beta Oligomers Neutralized by Sequestration. Cell Rep. 2015; 11:1760–1771. [PubMed: 26051935]

5. Guerreiro R, Wojtas A, Bras J, Carrasquillo M, Rogaeva E, Majounie E, Cruchaga C, Sassi C, Kauwe JS, Younkin S, Hazrati L, Collinge J, Pocock J, Lashley T, Williams J, Lambert JC, Amouyel P, Goate A, Rademakers R, Morgan K, Powell J, St George-Hyslop P, Singleton A, Hardy J. Alzheimer Genetic Analysis G. TREM2 variants in Alzheimer's disease. N Engl J Med. 2013; 368:117–127. [PubMed: 23150934]
6. Jonsson T, Stefansson H, Steinberg S, Jonsdottir I, Jonsson PV, Snaedal J, Bjornsson S, Huttenlocher J, Levey AI, Lah JJ, Rujescu D, Hampel H, Giegling I, Andreassen OA, Engedal K, Ulstein I, Djurovic S, Ibrahim-Verbaas C, Hofman A, Ikram MA, van Duijn CM, Thorsteinsdottir U, Kong A, Stefansson K. Variant of TREM2 associated with the risk of Alzheimer's disease. N Engl J Med. 2013; 368:107–116. [PubMed: 23150908]
7. Jay TR, Miller CM, Cheng PJ, Graham LC, Bemiller S, Broihier ML, Xu G, Margevicius D, Karlo JC, Sousa GL, Cotleur AC, Butovsky O, Bekris L, Staugaitis SM, Leverenz JB, Pimplikar SW, Landreth GE, Howell GR, Ransohoff RM, Lamb BT. TREM2 deficiency eliminates TREM2+ inflammatory macrophages and ameliorates pathology in Alzheimer's disease mouse models. J Exp Med. 2015; 212:287–295. [PubMed: 25732305]
8. Wang Y, Cella M, Mallinson K, Ulrich JD, Young KL, Robinette ML, Gilfillan S, Krishnan GM, Sudhakar S, Zinselmeyer BH, Holtzman DM, Cirrito JR, Colonna M. TREM2 lipid sensing sustains the microglial response in an Alzheimer's disease model. Cell. 2015; 160:1061–1071. [PubMed: 25728668]
9. Wang Y, Ulland TK, Ulrich JD, Song W, Tzaferis JA, Hole JT, Yuan P, Mahan TE, Shi Y, Gilfillan S, Cella M, Grutzendler J, DeMattos RB, Cirrito JR, Holtzman DM, Colonna M. TREM2-mediated early microglial response limits diffusion and toxicity of amyloid plaques. J Exp Med. 2016; 213:667–675. [PubMed: 27091843]
10. Jankowsky JL, Slunt HH, Ratovitski T, Jenkins NA, Copeland NG, Borchelt DR. Co-expression of multiple transgenes in mouse CNS: a comparison of strategies. Biomol Eng. 2001; 17:157–165. [PubMed: 11337275]
11. Oakley H, Cole SL, Logan S, Maus E, Shao P, Craft J, Guillozet-Bongaarts A, Ohno M, Disterhoft J, Van Eldik L, Berry R, Vassar R. Intraneuronal beta-amyloid aggregates, neurodegeneration, and neuron loss in transgenic mice with five familial Alzheimer's disease mutations: potential factors in amyloid plaque formation. J Neurosci. 2006; 26:10129–10140. [PubMed: 17021169]
12. Hsiao K, Chapman P, Nilsen S, Eckman C, Harigaya Y, Younkin S, Yang F, Cole G. Correlative memory deficits, Abeta elevation, and amyloid plaques in transgenic mice. Science. 1996; 274:99–102. [PubMed: 8810256]
13. Liu P, Paulson JB, Forster CL, Shapiro SL, Ashe KH, Zahs KR. Characterization of a novel mouse model of Alzheimer's disease-amyloid pathology and unique beta-amyloid oligomer profile. PLoS One. 2015; 10:e0126317. [PubMed: 25946042]
14. Li T, Braunstein KE, Zhang J, Lau A, Sibener L, Deeble C, Wong PC. The neuritic plaque facilitates pathological conversion of tau in an Alzheimer's disease mouse model. Nat Commun. 2016; 7:12082. [PubMed: 27373369]
15. Callahan MJ, Lipinski WJ, Bian F, Durham RA, Pack A, Walker LC. Augmented senile plaque load in aged female beta-amyloid precursor protein-transgenic mice. Am J Pathol. 2001; 158:1173–1177. [PubMed: 11238065]
16. Sadleir KR, Eimer WA, Cole SL, Vassar R. Abeta reduction in BACE1 heterozygous null 5XFAD mice is associated with transgenic APP level. Mol Neurodegener. 2015; 10:1. [PubMed: 25567526]
17. Lehman EJ, Kulnane LS, Gao Y, Petriello MC, Pimpis KM, Younkin L, Dolios G, Wang R, Younkin SG, Lamb BT. Genetic background regulates beta-amyloid precursor protein processing and beta-amyloid deposition in the mouse. Hum Mol Genet. 2003; 12:2949–2956. [PubMed: 14506131]
18. Lazarov O, Robinson J, Tang YP, Hairston IS, Korade-Mirnics Z, Lee VM, Hersh LB, Sapolsky RM, Mirnics K, Sisodia SS. Environmental enrichment reduces Abeta levels and amyloid deposition in transgenic mice. Cell. 2005; 120:701–713. [PubMed: 15766532]

19. Lewejohann L, Reefmann N, Widmann P, Ambree O, Herring A, Keyvani K, Paulus W, Sachser N. Transgenic Alzheimer mice in a semi-naturalistic environment: more plaques, yet not compromised in daily life. Behav Brain Res. 2009; 201:99–102. [PubMed: 19428622]
20. Nizari S, Carare RO, Hawkes CA. Increased Abeta pathology in aged Tg2576 mice born to mothers fed a high fat diet. Sci Rep. 2016; 6:21981. [PubMed: 26911528]
21. Herring A, Donath A, Yarmolenko M, Uslar E, Conzen C, Kanakis D, Bosma C, Worm K, Paulus W, Keyvani K. Exercise during pregnancy mitigates Alzheimer-like pathology in mouse offspring. FASEB J. 2012; 26:117–128. [PubMed: 21948247]
22. Itagaki S, McGeer PL, Akiyama H, Zhu S, Selkoe D. Relationship of microglia and astrocytes to amyloid deposits of Alzheimer disease. J Neuroimmunol. 1989; 24:173–182. [PubMed: 2808689]
23. Pike CJ, Cummings BJ, Cotman CW. Early association of reactive astrocytes with senile plaques in Alzheimer's disease. Exp Neurol. 1995; 132:172–179. [PubMed: 7789457]
24. Vehmas AK, Kawas CH, Stewart WF, Troncoso JC. Immune reactive cells in senile plaques and cognitive decline in Alzheimer's disease. Neurobiol Aging. 2003; 24:321–331. [PubMed: 12498966]
25. Knowles RB, Wyart C, Buldyrev SV, Cruz L, Urbanc B, Hasselmo ME, Stanley HE, Hyman BT. Plaque-induced neurite abnormalities: implications for disruption of neural networks in Alzheimer's disease. Proc Natl Acad Sci U S A. 1999; 96:5274–5279. [PubMed: 10220456]
26. Koffie RM, Meyer-Luehmann M, Hashimoto T, Adams KW, Mielke ML, Garcia-Alloza M, Micheva KD, Smith SJ, Kim ML, Lee VM, Hyman BT, Spires-Jones TL. Oligomeric amyloid beta associates with postsynaptic densities and correlates with excitatory synapse loss near senile plaques. Proc Natl Acad Sci U S A. 2009; 106:4012–4017. [PubMed: 19228947]
27. Meyer-Luehmann M, Spires-Jones TL, Prada C, Garcia-Alloza M, de Calignon A, Rozkalne A, Koenigsknecht-Talboo J, Holtzman DM, Bacskai BJ, Hyman BT. Rapid appearance and local toxicity of amyloid-beta plaques in a mouse model of Alzheimer's disease. Nature. 2008; 451:720–724. [PubMed: 18256671]
28. Spires TL, Meyer-Luehmann M, Stern EA, McLean PJ, Skoch J, Nguyen PT, Bacskai BJ, Hyman BT. Dendritic spine abnormalities in amyloid precursor protein transgenic mice demonstrated by gene transfer and intravital multiphoton microscopy. J Neurosci. 2005; 25:7278–7287. [PubMed: 16079410]
29. Spires-Jones TL, Meyer-Luehmann M, Osetek JD, Jones PB, Stern EA, Bacskai BJ, Hyman BT. Impaired spine stability underlies plaque-related spine loss in an Alzheimer's disease mouse model. Am J Pathol. 2007; 171:1304–1311. [PubMed: 17717139]
30. Su JH, Cummings BJ, Cotman CW. Plaque biogenesis in brain aging and Alzheimer's disease. I. Progressive changes in phosphorylation states of paired helical filaments and neurofilaments. Brain Res. 1996; 739:79–87. [PubMed: 8955927]
31. Busche MA, Eichhoff G, Adelsberger H, Abramowski D, Wiederhold KH, Haass C, Staufenbiel M, Konnerth A, Garaschuk O. Clusters of hyperactive neurons near amyloid plaques in a mouse model of Alzheimer's disease. Science. 2008; 321:1686–1689. [PubMed: 18802001]
32. Kuchibhotla KV, Goldman ST, Lattarulo CR, Wu HY, Hyman BT, Bacskai BJ. Abeta plaques lead to aberrant regulation of calcium homeostasis in vivo resulting in structural and functional disruption of neuronal networks. Neuron. 2008; 59:214–225. [PubMed: 18667150]
33. Kuchibhotla KV, Lattarulo CR, Hyman BT, Bacskai BJ. Synchronous hyperactivity and intercellular calcium waves in astrocytes in Alzheimer mice. Science. 2009; 323:1211–1215. [PubMed: 19251629]
34. Serrano-Pozo A, Muzikansky A, Gomez-Isla T, Growdon JH, Betensky RA, Frosch MP, Hyman BT. Differential relationships of reactive astrocytes and microglia to fibrillar amyloid deposits in Alzheimer disease. J Neuropathol Exp Neurol. 2013; 72:462–471. [PubMed: 23656989]
35. Mitew S, Kirkcaldie MT, Dickson TC, Vickers JC. Neurites containing the neurofilament-triplet proteins are selectively vulnerable to cytoskeletal pathology in Alzheimer's disease and transgenic mouse models. Front Neuroanat. 2013; 7:30. [PubMed: 24133416]
36. Riley KP, Snowdon DA, Markesbery WR. Alzheimer's neurofibrillary pathology and the spectrum of cognitive function: findings from the Nun Study. Ann Neurol. 2002; 51:567–577. [PubMed: 12112102]

37. Snowdon DA, Greiner LH, Mortimer JA, Riley KP, Greiner PA, Markesbery WR. Brain infarction and the clinical expression of Alzheimer disease. The Nun Study. Jama. 1997; 277:813–817. [PubMed: 9052711]
38. Ruan L, Kang Z, Pei G, Le Y. Amyloid deposition and inflammation in APPswe/PS1dE9 mouse model of Alzheimer's disease. Curr Alzheimer Res. 2009; 6:531–540. [PubMed: 19747158]
39. Rees T, Hammond PI, Soreq H, Younkin S, Brimijoin S. Acetylcholinesterase promotes beta-amyloid plaques in cerebral cortex. Neurobiol Aging. 2003; 24:777–787. [PubMed: 12927760]
40. Jankowsky JL, Fadale DJ, Anderson J, Xu GM, Gonzales V, Jenkins NA, Copeland NG, Lee MK, Younkin LH, Wagner SL, Younkin SG, Borchelt DR. Mutant presenilins specifically elevate the levels of the 42 residue beta-amyloid peptide in vivo: evidence for augmentation of a 42-specific gamma secretase. Hum Mol Genet. 2004; 13:159–170. [PubMed: 14645205]
41. Kawarabayashi T, Younkin LH, Saido TC, Shoji M, Ashe KH, Younkin SG. Age-dependent changes in brain, CSF, and plasma amyloid ß protein in the Tg2576 transgenic mouse model of Alzheimer's disease. Journal of Neuroscience. 2001; 21:372–381. [PubMed: 11160418]
42. Alzforum, Mutations. http://www.alzforum.org/mutations.
43. Dinkins MB, Dasgupta S, Wang G, Zhu G, He Q, Kong JN, Bieberich E. The 5XFAD Mouse Model of Alzheimer's Disease Exhibits an Age-Dependent Increase in Anti-Ceramide IgG and Exogenous Administration of Ceramide Further Increases Anti-Ceramide Titers and Amyloid Plaque Burden. J Alzheimers Dis. 2015; 46:55–61. [PubMed: 25720409]
44. Ou-Yang MH, Xu F, Liao MC, Davis J, Robinson JK, Van Nostrand WE. N-terminal region of myelin basic protein reduces fibrillar amyloid-beta deposition in Tg-5xFAD mice. Neurobiol Aging. 2015; 36:801–811. [PubMed: 25457550]
45. Condello C, Yuan P, Schain A, Grutzendler J. Microglia constitute a barrier that prevents neurotoxic protofibrillar Abeta42 hotspots around plaques. Nat Commun. 2015; 6:6176. [PubMed: 25630253]
46. Snellman A, Lopez-Picon FR, Rokka J, Salmona M, Forloni G, Scheinin M, Solin O, Rinne JO, Haaparanta-Solin M. Longitudinal amyloid imaging in mouse brain with 11C-PIB: comparison of APP23, Tg2576, and APPswe-PS1dE9 mouse models of Alzheimer disease. J Nucl Med. 2013; 54:1434–1441. [PubMed: 23833271]
47. Garcia-Alloza M, Robbins EM, Zhang-Nunes SX, Purcell SM, Betensky RA, Raju S, Prada C, Greenberg SM, Bacskai BJ, Frosch MP. Characterization of amyloid deposition in the APPswe/PS1dE9 mouse model of Alzheimer disease. Neurobiol Dis. 2006; 24:516–524. [PubMed: 17029828]
48. Bolmont T, Haiss F, Eicke D, Radde R, Mathis CA, Klunk WE, Kohsaka S, Jucker M, Calhoun ME. Dynamics of the microglial/amyloid interaction indicate a role in plaque maintenance. J Neurosci. 2008; 28:4283–4292. [PubMed: 18417708]
49. Yan P, Bero AW, Cirrito JR, Xiao Q, Hu X, Wang Y, Gonzales E, Holtzman DM, Lee JM. Characterizing the appearance and growth of amyloid plaques in APP/PS1 mice. J Neurosci. 2009; 29:10706–10714. [PubMed: 19710322]
50. Burgold S, Bittner T, Dorostkar MM, Kieser D, Fuhrmann M, Mitteregger G, Kretzschmar H, Schmidt B, Herms J. In vivo multiphoton imaging reveals gradual growth of newborn amyloid plaques over weeks. Acta Neuropathol. 2011; 121:327–335. [PubMed: 21136067]
51. Hefendehl JK, Wegenast-Braun BM, Liebig C, Eicke D, Milford D, Calhoun ME, Kohsaka S, Eichner M, Jucker M. Long-term in vivo imaging of beta-amyloid plaque appearance and growth in a mouse model of cerebral beta-amyloidosis. J Neurosci. 2011; 31:624–629. [PubMed: 21228171]
52. Christie RH, Bacskai BJ, Zipfel WR, Williams RM, Kajdasz ST, Webb WW, Hyman BT. Growth arrest of individual senile plaques in a model of Alzheimer's disease observed by in vivo multiphoton microscopy. J Neurosci. 2001; 21:858–864. [PubMed: 11157072]
53. Ingelsson M, Fukumoto H, Newell KL, Growdon JH, Hedley-Whyte ET, Frosch MP, Albert MS, Hyman BT, Irizarry MC. Early Abeta accumulation and progressive synaptic loss, gliosis, and tangle formation in AD brain. Neurology. 2004; 62:925–931. [PubMed: 15037694]

54. Woodhouse A, Shepherd CE, Sokolova A, Carroll VL, King AE, Halliday GM, Dickson TC, Vickers JC. Cytoskeletal alterations differentiate presenilin-1 and sporadic Alzheimer's disease. Acta Neuropathol. 2009; 117:19–29. [PubMed: 19015863]

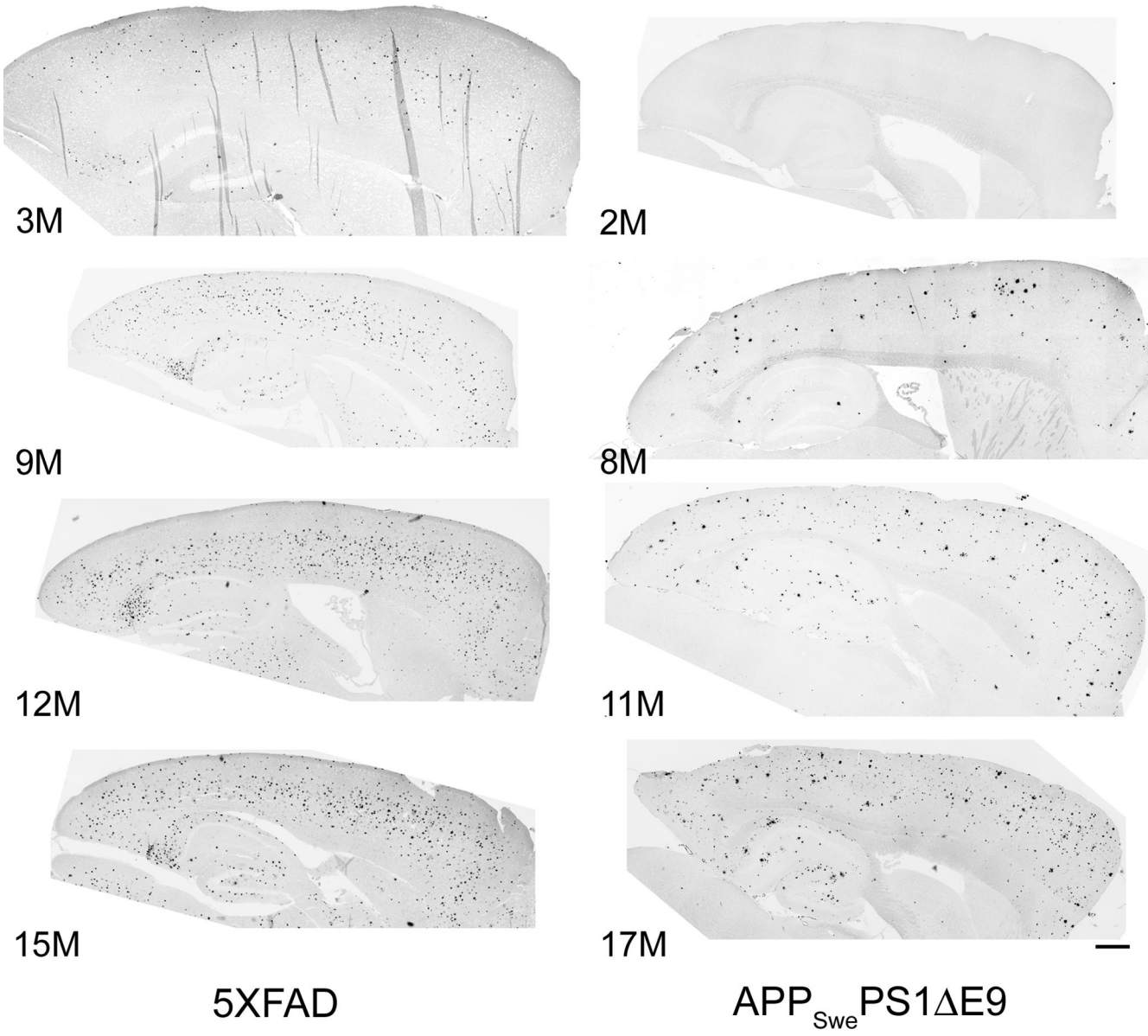

Fig. 1. Age-dependent plaque deposition in female 5XFAD and male $APP_{Swe}PS1\Delta E9$ mice

Photomicrographs of sagittal sections stained with Thioflavin S, to label dense-core plaques. Images were collected on a Nikon TiE deconvolution microscope with a 10× objective, then tiled to show complete sections. Images are shown with contrast inverted. Numbers indicate ages of mice (in months); dorsal is up, anterior is to the right. Scale bar, 500 μm.

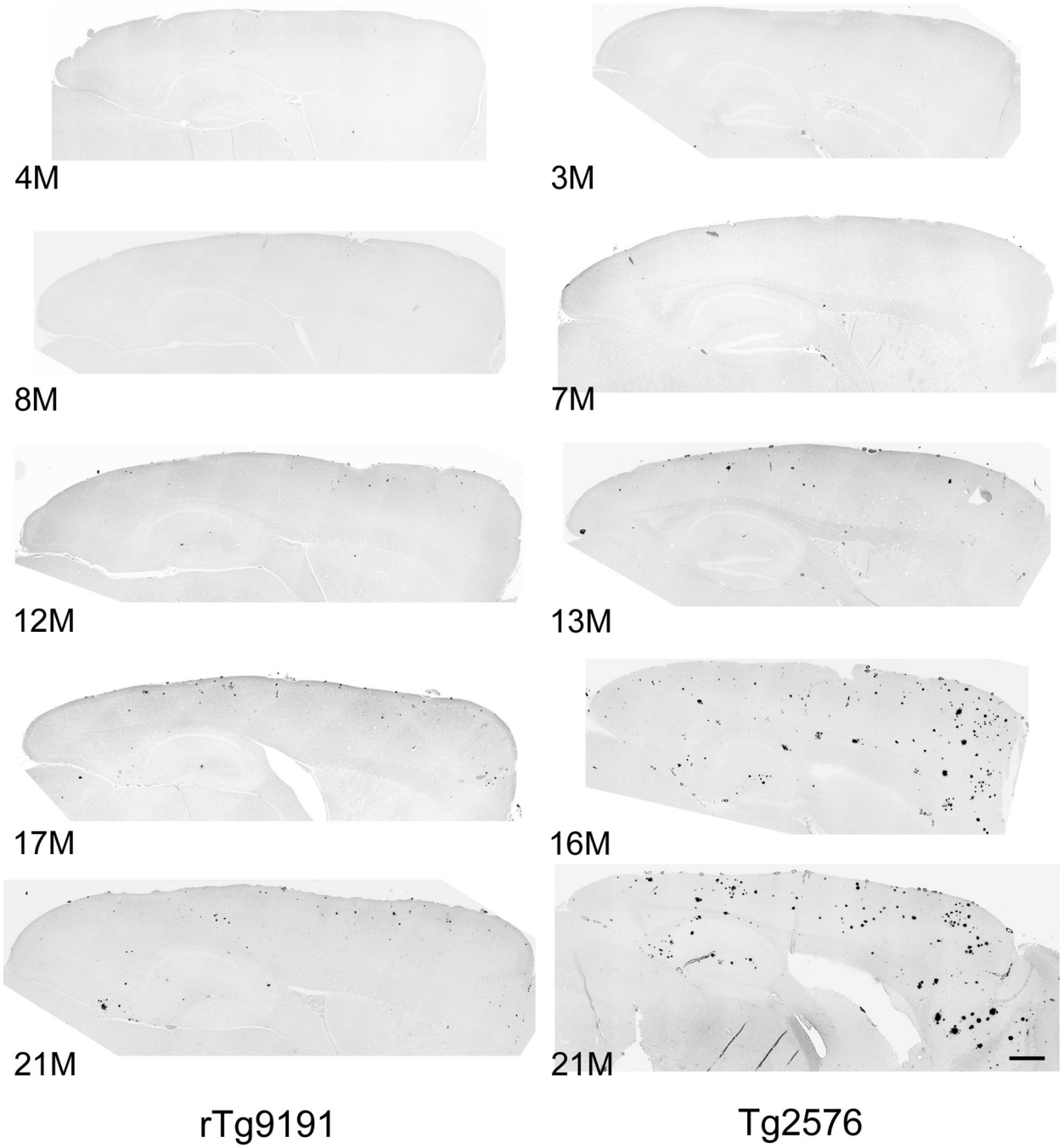

Fig. 2. Age-dependent plaque deposition in male rTg9191 and Tg2576 mice

Photomicrographs of sagittal sections stained with Thioflavin S, to label dense-core plaques. Images were collected on a Nikon TiE deconvolution microscope with a 10× objective, then tiled to show complete sections. Images are shown with contrast inverted. Numbers indicate ages of mice (in months); dorsal is up, anterior is to the right. Scale bar, 500 μm.

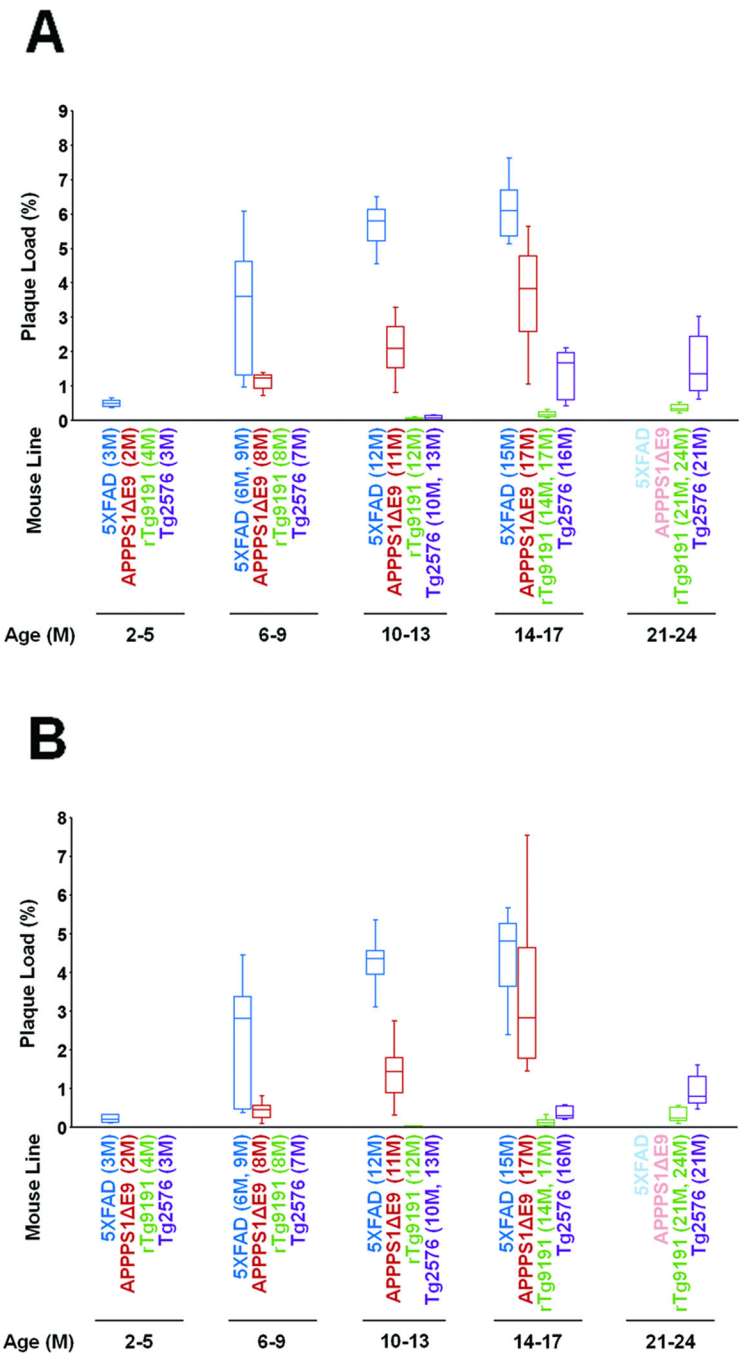

Fig. 3. Quantification of dense-core (Thioflavin S-reactive) plaque burdens

The Thioflavin S plaque burden was calculated as the sum of the area of all Thioflavin S-reactive plaques divided by the total sampled area of cerebral cortex or hippocampal formation. (**A**) Cortex. (**B**) Hippocampus. Box plots show median, interquartile ranges, and minima and maxima for each line at each age evaluated. Note that $APP_{Swe}PS1\Delta E9$ are labeled “APPPS1ΔE9” and that no data were available from 5XFAD or $APP_{Swe}PS1\Delta E9$ at 21-24 months of age.

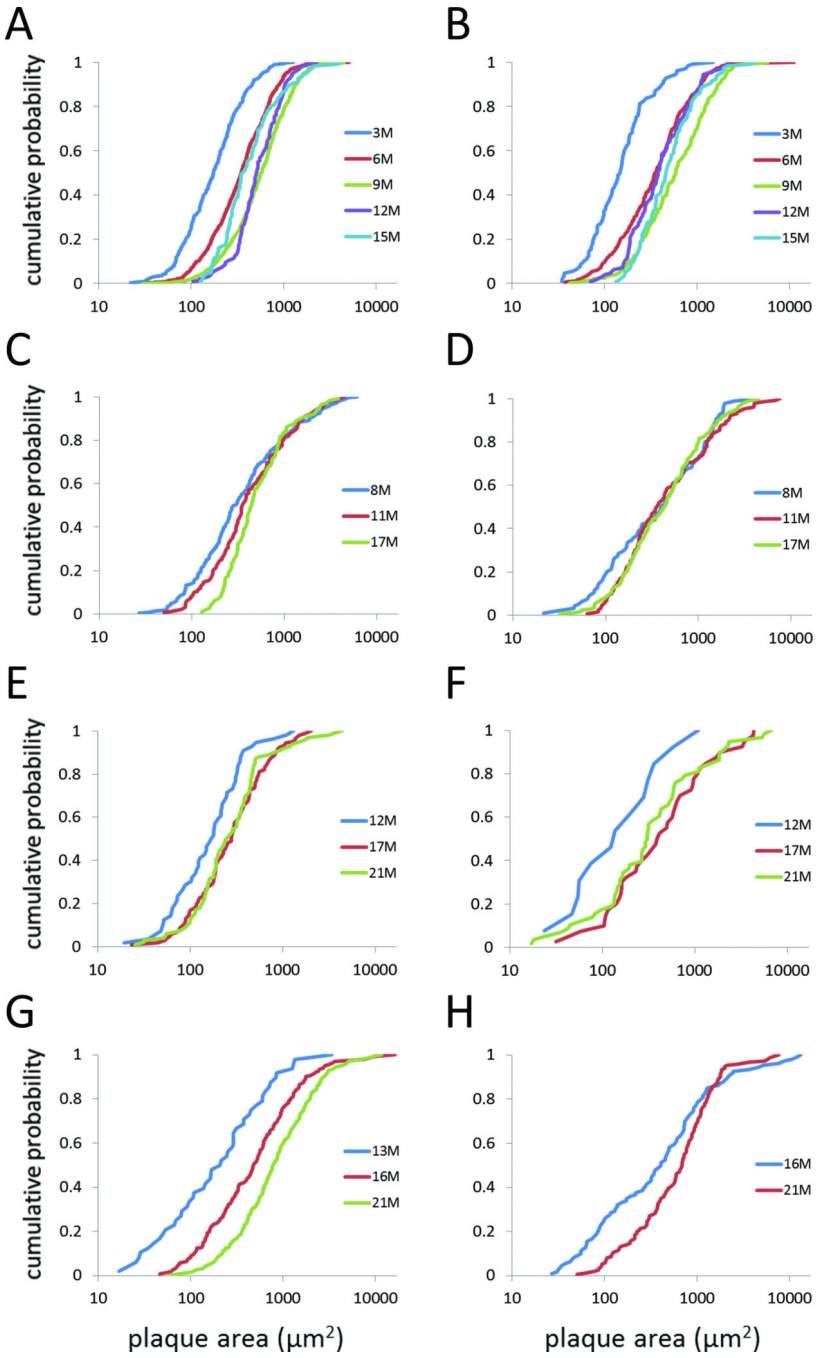

Fig. 4. Plaque-size distributions as a function of age, within lines

Plaque-size distributions are represented as cumulative probability plots. (**A, B**) 5XFAD. (**C, D**) $APP_{Swe}PS1\Delta E9$. (**E, F**) rTg9191. (**G, H**) Tg2576. Left column (A, C, E, G), cortex; right column (B, D, F, H), hippocampus. Data are from female 5XFAD mice, male $APP_{Swe}PS1\Delta E9$, rTg9191, and Tg2576 mice.

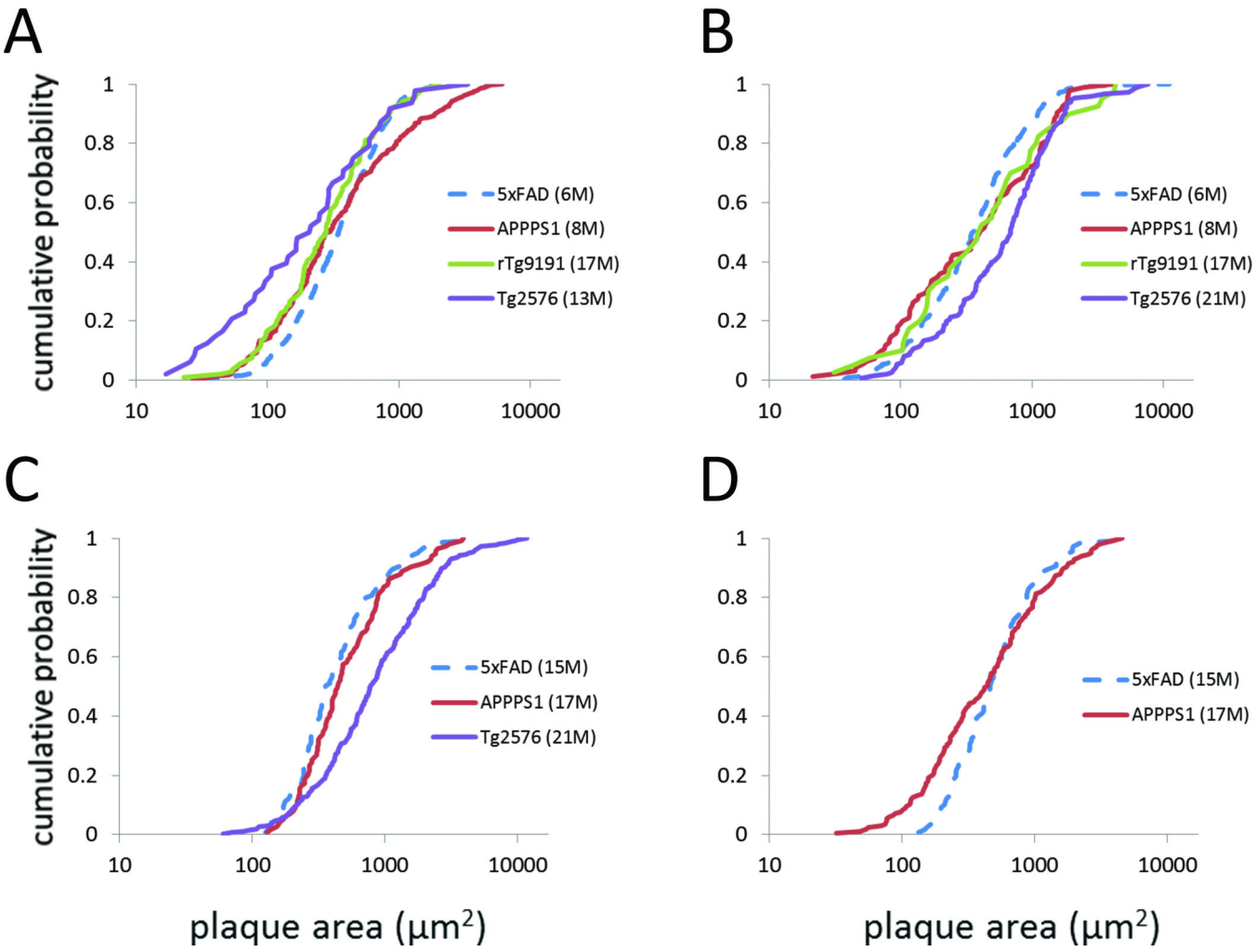

Fig. 5. Inter-line comparison of plaque-size distributions, based on duration of plaque deposition

Thioflavin-S plaque-area distributions, represented as cumulative probability plots, after 4±1 (**A, B**) or 12±1 (**C, D**) months of plaque deposition. (A, C) cortex; (B, D) hippocampus. Dashed lines indicate that data are from female 5XFAD mice; only male mice contributed data for the other lines. Note that $APP_{Swe}PS1\Delta E9$ are labeled "APPPS1."

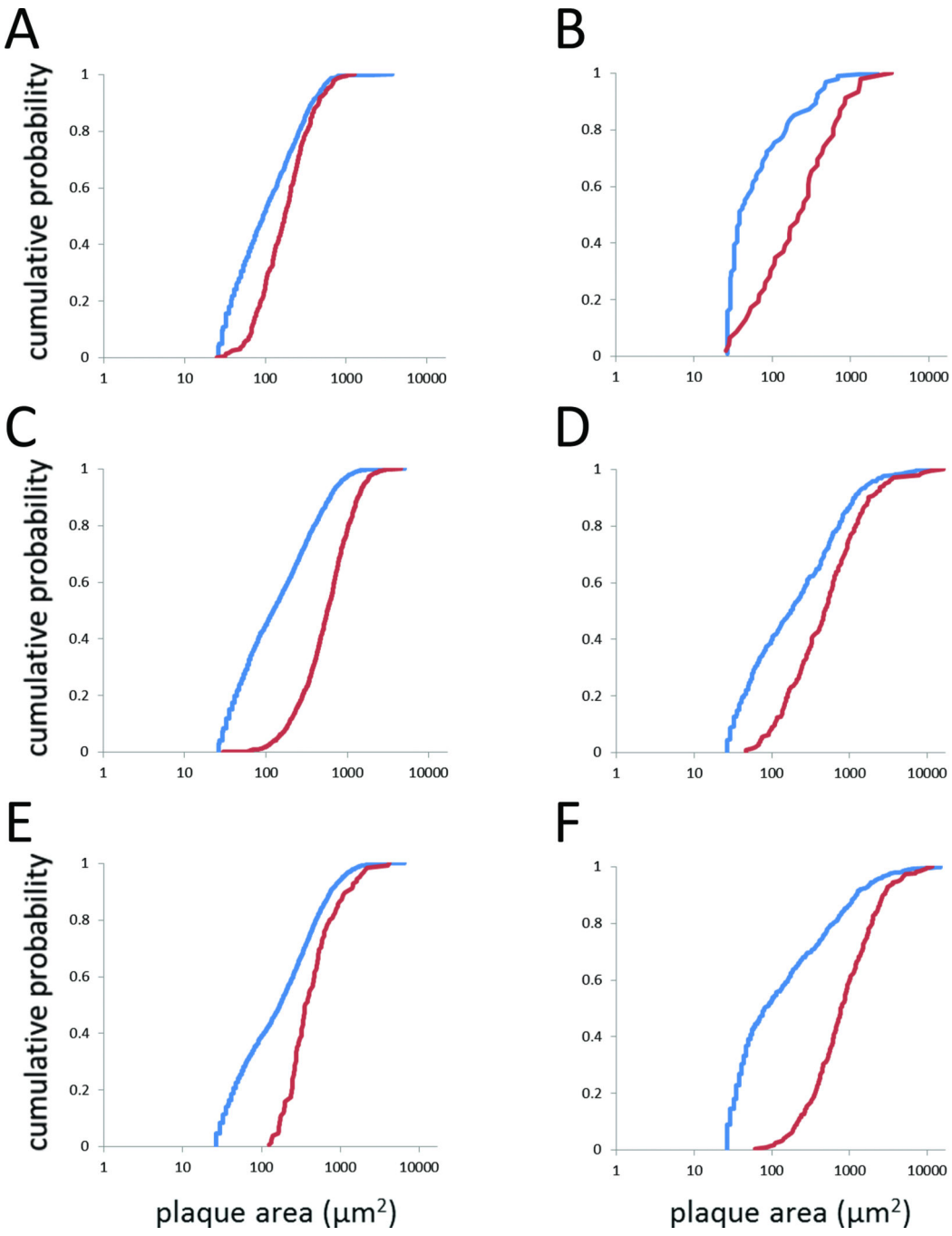

Fig. 6. Comparison of methods for measuring plaque sizes

Plaque size distributions obtained by viewing sections at higher magnification and measuring cortical plaque areas with Stereo Investigator (red) or by automated measurements on low-magnification images using ImageJ (blue). Only objects > 35 μm^2 were included in this analysis. Six examples are shown, including sections with relatively high plaque burdens (5XFAD) and low-to-moderate plaque burdens (Tg2576). (**A**) 3M 5XFAD. (**B**) 13M Tg2576. (**C**) 9M 5XFAD. (**D**) 16M Tg2576. (**E**) 15M 5XFAD. (**F**) 21M Tg2576. In all cases, the distributions obtained by the two methods differed significantly

(Kolmogorov-Smirnov test: $p = 0.009$ for 13M Tg2576, $p < 0.006$ for all other pairwise comparison, corrected for multiple comparisons).

Table 1

Mouse lines.

Mouse line	Background strain	Transgene(s)	Ages studied (months)
5XFAD, line 6799	C57Bl6 X SJL (F2)	*AβPP*$_{695}$ with K670N/M671L (Swedish), I716V (Florida), and V717I (London) mutations; *PSEN1* with M146L and L286V mutations; driven by the *THY1* promoter	3, 6, 9, 12, 15
APP$_{Swe}$PS1ΔE9, line 85	C57Bl6 X C3H (F2)	*AβPP*$_{695}$ with K670N/M671L (Swedish) mutation; *PSEN1* with deletion of exon 9; driven by the *PRNP* promoter	2, 8, 11, 17
rTg9191	129 X FVB	*AβPP*$_{695}$ with K670N/M671L (Swedish) and V717I (London) mutations; regulatable – transactivator driven by the *CaMKII* promoter	4, 8, 12, 14, 17, 21, 24
Tg2576	C57Bl6 X SJL (F2)	*AβPP*$_{695}$ with K670N/M671L (Swedish) mutation; driven by the *PRNP* promoter	3, 7, 10, 13, 16, 21

AβPP, amyloid-β precursor protein; *CaMKII*, calcium-calmodulin kinase, type 2; *PRNP*, cellular prion protein; *PSEN1*, presenilin-1.

Table 2

Human subjects

			Dense-core plaque burden[a]			
Braak Stage	**Age (yr)**	**Mean cortical plaque count[b]**	**Frontal lobe**	**Superior and middle temporal gyrus**	**Inferior parietal lobe**	**Composite cortical plaque burden[c]**
5	92	15.09	0.25% (3)	0.54% (4)	0.30% (4)	0.37 ± 0.17%
6	95	14.38	0.37% (3)	0.17% (3)	0.49% (4)	0.36 ± 0.19%
6	92	7.86	0.10% (3)	0.06% (2)	0.08% (4)	0.08 ± 0.06%
5	91	6.87	0.06% (3)	0.03% (4)	0.08% (4)	0.06 ± 0.06%
6	94	4.96	0.03% (2)	0.11% (3)	0.17% (3)	0.12 ± 0.10%
6	90	4.40	0.09% (3)	0.08% (3)	0.04% (4)	0.07 ± 0.04%

[a] Mean plaque burden calculated from all sampled sections/region/subject; number in parentheses = number of sections sampled.

[b] Mean number of neuritic plaques/mm^2 in sections of frontal lobe (area 9), superior and middle temporal gyrus, and inferior parietal lobe.

[c] Mean ± std. dev., all sections sampled.

Table 3

Comparison of plaque burdens as a function of age, within lines (p values)

5XFAD	Kruskal-Wallis: cortex <0.0001; hippocampus <0.0001				
	2–5M	**6–9M**	**10–13M**	**14–17M**	**21–24M**
2–5M	--	0.004	0.011	0.011	n.d.
6–9M	0.004	--	0.013	0.003	n.d.
10–13M	0.011	0.011	--	(>0.9999)	n.d.
14–17M	0.011	0.020	(>0.9999)	--	n.d.
21–24M	n.d.	n.d.	n.d.	n.d.	--
$APP_{Swe}PS1\Delta E9$	Kruskal-Wallis: cortex <0.0001; hippocampus <0.0001				
	2–5M	**6–9M**	**10–13M**	**14–17M**	**21–24M**
2–5M	--	<0.0006	<0.0006	<0.0006	n.d.
6–9M	<0.0006	--	<0.0006	<0.0006	n.d.
10–13M	<0.0006	<0.0006	--	<0.0018	n.d.
14–17M	<0.0006	<0.0006	<0.0006	--	n.d.
21–24M	n.d.	n.d.	n.d.	n.d.	--
rTg9191	Kruskal-Wallis: cortex <0.0001; hippocampus <0.0001				
	2–5M	**6–9M**	**10–13M**	**14–17M**	**21–24M**
2–5M	--	N.A.	0.03	<0.001	<0.001
6–9M	N.A.	--	0.03	<0.001	<0.001
10–13M	0.03	0.03	--	0.009	0.004
14–17M	<0.001	<0.001	0.003	--	0.004
21–24M	<0.001	<0.001	0.004	(0.071)	--
Tg2576	Kruskal-Wallis: cortex <0.0001; hippocampus <0.0001				
	2–5M	**6–9M**	**10–13M**	**14–17M**	**21–24M**
2–5M	--	N.A.	0.015	0.025	0.011
6–9M	N.A.	--	0.015	0.025	0.011
10–13M	N.A.	N.A.	--	0.008	0.001
14–17M	0.019	0.019	0.0005	--	(>0.9999)
21–24M	0.009	0.009	0.0002	0.027	--

Non-parametric analysis of variance (Kruskal-Wallis test), followed by Mann-Whitney test. P values were adjusted for multiple comparisons using the Bonferroni method. Open boxes, cortex; shaded boxes, hippocampus.

(), not significant with $\alpha = 0.05$; n.d., data not available; N.A., not applicable.

Ages were binned into 4-5-month spans in order to facilitate comparisons between lines, which were studied at different ages. Exact ages studied for each line are shown in Table 1.

Table 4

Inter-line comparison of plaque burdens, based on duration of plaque deposition (p values)

4±1 M	Kruskal-Wallis: cortex 0.0001; hippocampus 0.0001			
	5XFAD	**APP$_{Swe}$PS1ΔE9**	**rTg9191**	**Tg2576**
5XFAD	--	(>0.9999)	0.0132	0.0132
APP$_{Swe}$PS1ΔE9	(>0.9999)	--	0.0024	0.0024
rTg9191	0.0132	(0.216)	--	(0.3504)
Tg2576	0.0456	0.0168	0.0024	--
12±1 M	Kruskal-Wallis: cortex <0.0001; hippocampus[a]			
	5XFAD	**APP$_{Swe}$PS1ΔE9**	**rTg9191**	**Tg2576**
5XFAD	--	0.0003	n.d.	0.0003
APP$_{Swe}$PS1ΔE9	(0.0856)	--	n.d.	0.0024
rTg9191	n.d.	n.d.	--	n.d.
Tg2576	n.d.	n.d.	n.d.	--

Non-parametric analysis of variance (Kruskal-Wallis test), followed by Mann-Whitney test, corrected for multiple comparisons.

[a]Mann-Whitney test only. Open boxes, cortex; shaded boxes, hippocampus.

() not significant with $\alpha = 0.05$; n.d., data not available.

Table 5

Comparison of plaque sizes as a function of age, within lines (p values)

5XFAD	**3M**	**6M**	**9M**	**12M**	**15M**
3M	--	<0.0001	<0.0001	<0.0001	<0.0001
6M	<0.0001	--	<0.001	<0.0001	(0.1)
9M	<0.001	<0.001	--	(>0.9999)	<0.001
12M	<0.0001	(0.7)	0.002	--	<0.0001
15M	<0.0001	0.04	(0.157)	(>0.9999)	--
$APP_{Swe}PS1\Delta E9$	**8M**	**11M**	**17M**		
8M	--	(0.1164)	<0.0006		
11M	(>0.9999)	--	(0.2154)		
17M	(0.7182)	(>0.9999)	--		
rTg9191	**12M**	**17M**	**21M**		
12M	--	(0.057)	(0.068)		
17M	(0.552)	--	(>0.9999)		
21M	(>0.9999)	(>0.9999)	--		
Tg2576	**13M**	**16M**	**21M**		
13M	--	0.003	<0.0001		
16M	n.d.	--	<0.0001		
21M	n.d.	0.005	--		

Kolmogorov-Smirnov test, corrected for multiple comparisons. Open boxes, cortex; shaded boxes, hippocampus.

() not significant with $\alpha = 0.05$; n.d., data not available.

Table 6

Inter-line comparison of plaque sizes, based on duration of plaque deposition (p values)

4±1 M	**5XFAD**	**APP$_{Swe}$PS1ΔE9**	**rTg9191**	**Tg2576**
5XFAD	--	0.0084	(0.1452)	0.0054
APP$_{Swe}$PS1ΔE9	(0.2844)	--	(0.6306)	(0.2526)
rTg9191	(>0.9999)	(>0.9999)	--	(0.7428)
Tg2576	<0.0006	(0.0732)	(0.8454)	--
12±1 M	**5XFAD**	**APP$_{Swe}$PS1ΔE9**	**rTg9191**	**Tg2576**
5XFAD	--	(0.5697)	n.d.	<0.0003
APP$_{Swe}$PS1ΔE9	0.0084	--	n.d.	<0.0003
rTg9191	n.d.	n.d.	--	n.d.
Tg2576	n.d.	n.d.	n.d.	--

Kolmogorov-Smirnov test, corrected for multiple comparisons. Open boxes, cortex; shaded boxes, hippocampus.

() not significant with $\alpha = 0.05$; n.d. data not available.